

CHEMPHYSICHEM

Supporting Information

© Copyright Wiley-VCH Verlag GmbH & Co. KGaA, 69451 Weinheim, 2013

A Rapid Freeze-Quench Setup for Multi-Frequency EPR Spectroscopy of Enzymatic Reactions

Roberta Pievo,^{*[a]} Brigitta Angerstein,^[a] Alistair J. Fielding,^[a, b] Christian Koch,^[c] Ivo Feussner,^[c] and Marina Bennati^{*[a, d]}

cphc_201300714_sm_miscellaneous_information.pdf

Supporting Information

Table of Contents	Page
Absorbance Spectroscopy Measurements on the 2,4-dinitrophenyl acetate hydrolysis	S2
Stopped-flow kinetics of the binding reaction of myoglobin with sodium azide	S3-S4
Derivation of parameter $h(t)$	S5-S6
Sample collectors for X- and Q-band EPR	S7
Sample collector for W-band EPR	S8
Comparison of the 9.4 GHz-EPR spectra of the RFQ samples of the reaction between PpoA and (<i>8R</i>)-HPODE, prepared in W-band tubes	S9
9.4 GHz EPR spectra of the RFQ samples of the reaction between PpoA and (<i>8R</i>)-HPODE, prepared in different EPR tubes	S10
References	S10

Absorbance Spectroscopy Measurements

Spectra were acquired on a Cary 100 UV-Vis spectrophotometer (Varian) using 700 μl cuvettes made in quartz SUPRASIL[®] with a 10 mm optical path. A solvent spectrum was used as blank. For kinetic studies on the hydrolysis of DNPA with NaOH, reaction samples (300 μl) with different ageing times were prepared using the micro-mix SFM-20 apparatus (Bio-Logic) and quenched in 300 μl of 3 M HCl. The initial concentration of DNPA was 1 mM (1% (v/v) DMSO, 2 mM HCl) and NaOH was used as 0.2 M solution. The reaction was performed at 23 °C and the kinetic measurements were repeated in triplicates. The formation of 2,4-dinitrophenol (DNP) was followed at 325 nm. The data were fitted using the mono-exponential model based on the following equation:^[1]

$$A_t = A_\infty + (A_0 - A_\infty) \times e^{-k't}$$

where A_t is the absorption intensity as a function of time (t); A_0 and A_∞ are the absorption intensities of the sample at time $t = 0$ and at completion of the reaction, respectively; k' is the apparent reaction rate constant. All the curves were satisfactory fitted to this model ($R^2 > 0.997$).

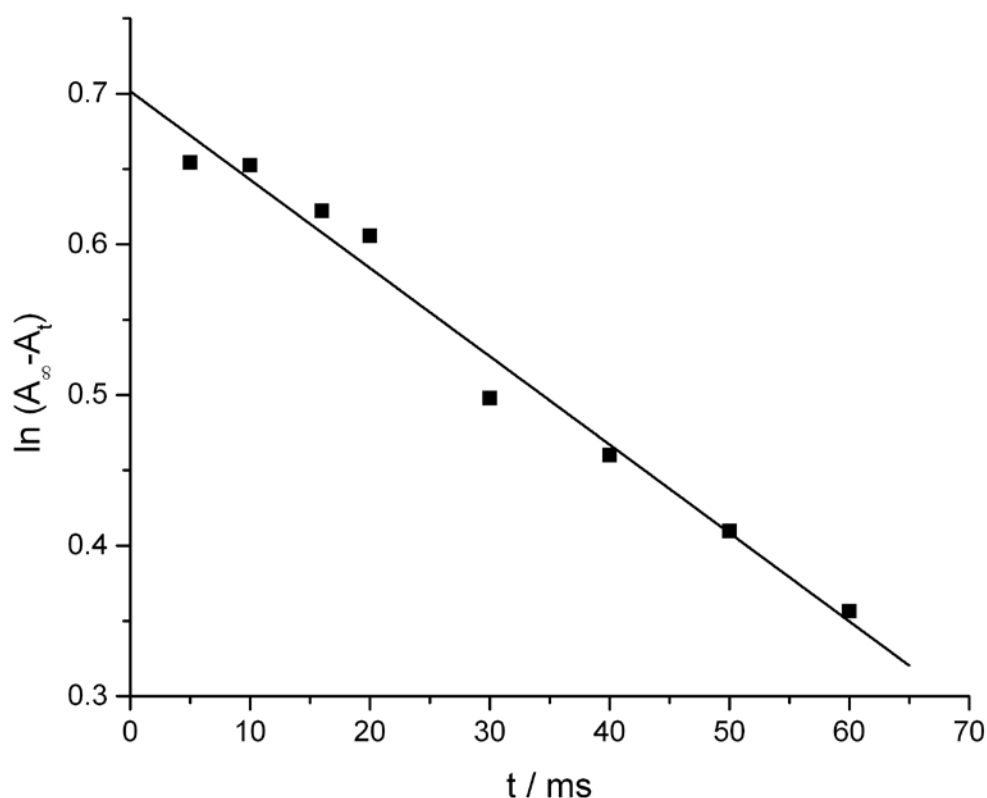


Figure S1: Semilogarithmic plot of the rate of hydrolysis of 2,4-dinitrophenyl acetate with NaOH.

Stopped flow experiments with myoglobin and sodium azide

A series of stopped-flow measurements on the reaction of myoglobin (Mb) with sodium azide were performed to determine the rate constant of the reaction for a direct comparison with the values obtained from the RFQ experiments carried out under the same conditions (pH, temperature). The binding of azide to the myoglobin was studied by following the change in the absorption signal at 575 nm with the time, that corresponds to the formation of the Mb-azide complex.^[2] The traces exhibited pseudo-first order kinetics over the range of azide concentration used (Fig S2). The data were well fitted using a mono-exponential model, from which the apparent rate constants k' were determined. The plot of k' vs. the concentration of azide showed a linear behavior, and from the fitting a rate constant k of $6504 (\pm 49) \text{ M}^{-1} \text{ s}^{-1}$ was found. This value is in good agreement with literature values for similar experimental conditions.^[3]

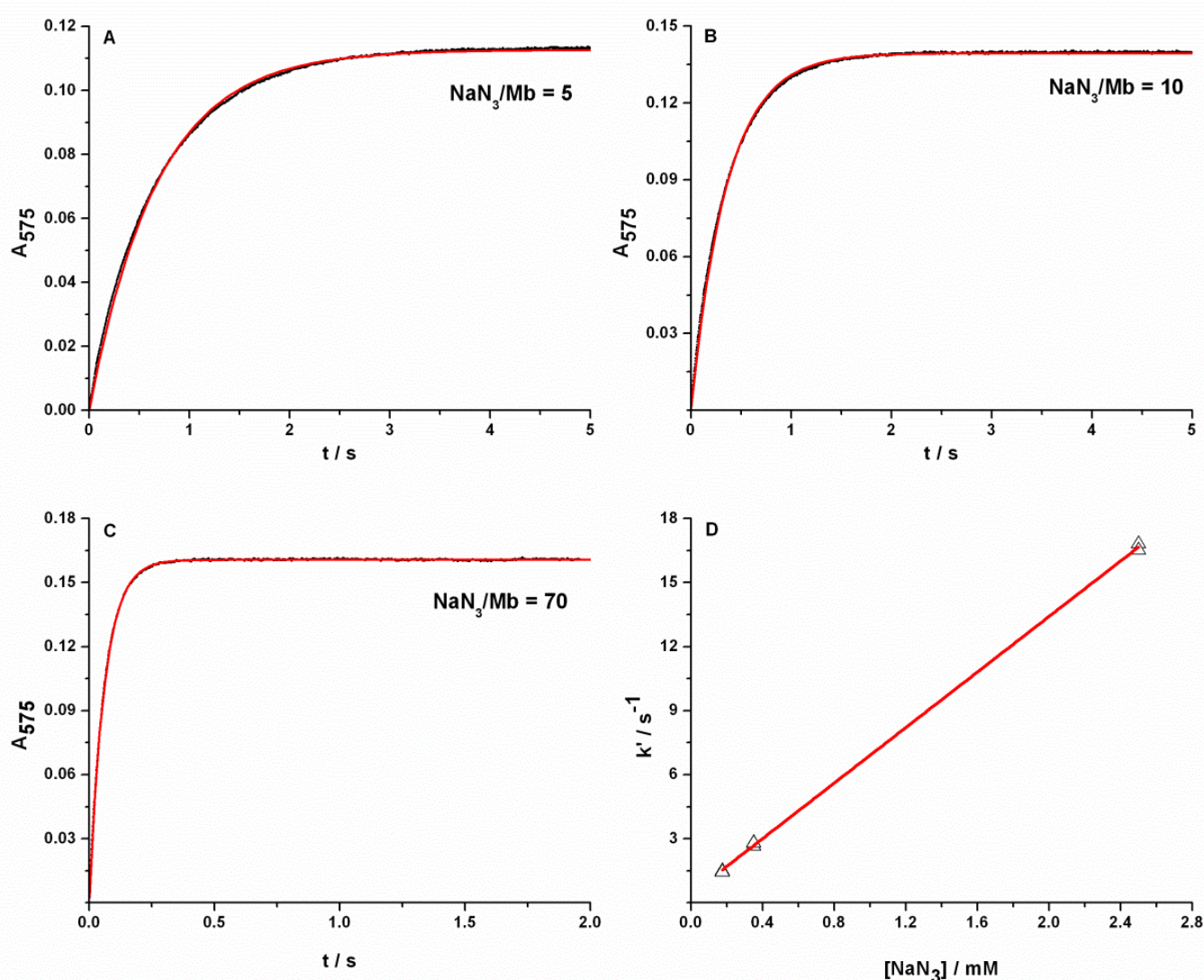


Figure S2: A-C: kinetic data for reaction between myoglobin and sodium azide, at different azide-to-myoglobin ratios. Absorbance changes at 575 nm (black squares) were followed by stopped-flow measurements. The solid red lines show mono-exponential fit to the data; D: pseudo-first order rate constants as a function of the concentration of sodium azide (open triangles) and linear fit (solid red line).

All kinetic measurements were performed at 23 °C using an SX.18MV stopped-flow system (Applied Photophysics). The dead time of the device was 2 ms. For measurements of the kinetics of myoglobin (70 μM) with sodium azide (0.35, 0.70 and 5 mM), equal volumes of the reagents solutions were mixed to give a final protein concentration of 35 μM and an azide-to-Mb ratio of 5, 10 and 70, respectively. The binding kinetics of the reaction was studied following the formation of the Mb-azide complex at 575 nm.^[2] The kinetic measurements for each azide-to-Mb ratio were repeated at least three times. Data were fitted using the mono-exponential model based on the following equation:

$$A(t) = c \times (1 - e^{-k't})$$

where $A(t)$ is the absorption intensity as a function of time (t); c is a constant given by $c = \epsilon \times b \times [\text{Mb}]_0$ (ϵ is the molar absorption coefficient, b is the cell path length, $[\text{Mb}]_0$ is concentration of Mb at time $t = 0$) and k' is the apparent reaction rate constant. All the curves were satisfactorily fitted to this model ($R^2 > 0.998$). The reaction rate constant k for the binding of azide to the myoglobin was determined by linear fitting of the plot k' vs. azide concentration ($k' = k [\text{NaN}_3]$).

Derivation of h(t)

Considering the conversion of the high-spin (HS) to the low spin (LS) form of myoglobin (Mb), mediated by sodium azide, NaN_3 , the reaction follows a 2nd order kinetic:



When azide is used in excess in respect to Mb, its concentration can be considered constant during the process and the reaction follows a pseudo-1st order kinetic. Under this condition, Eq. 1 can be restated as:

$$v = -k' \times [\text{HS}] \quad (2)$$

Giving the integrated pseudo-1st-order rate law:

$$\frac{[\text{HS}]_t}{[\text{HS}]_0} = e^{-k't} \quad (3)$$

Where k' is defined as the apparent kinetic constant: $k' = k \times [\text{N}_3^-]$ (4)

Since the concentration of a species is proportional to its double integrated 1st-derivative EPR signal, we have:

$$[\text{HS}]_t = a \times (A_{\text{HS}})_t \quad (4)$$

$$[\text{LS}]_t = b \times (A_{\text{LS}})_t \quad (5)$$

Where A is defined as the double integrated intensity of the EPR signal, a and b are the proportionality factors.

Eq. 3 can be restated as a function of the double-integrated EPR signals:

$$\frac{[\text{HS}]_t}{[\text{HS}]_0} = \frac{a \times (A_{\text{HS}})_t}{a \times (A_{\text{HS}})_0} = e^{-k' \times t} \Rightarrow \frac{(A_{\text{HS}})_t}{(A_{\text{HS}})_0} = e^{-k' \times t} \quad (6)$$

The initial concentration of HS-Mb is equal to the concentration of LS-Mb at the end of the reaction:

$$[\text{HS}]_0 = [\text{LS}]_{\text{fin}} \quad (7)$$

From this equivalence, it is possible to define the parameter R_0 :

$$a \times (A_{\text{HS}})_0 = b \times (A_{\text{LS}})_{\text{fin}} \Rightarrow \frac{(A_{\text{HS}})_0}{(A_{\text{LS}})_{\text{fin}}} = \frac{b}{a} = R_0 \quad (8)$$

And the parameter R_t :

$$R_t = \frac{(A_{\text{HS}})_t}{(A_{\text{LS}})_t} \Rightarrow R_t = \frac{[\text{HS}]_t}{a} \times \frac{b}{[\text{LS}]_t} = R_0 \times \frac{[\text{HS}]_t}{[\text{LS}]_t} \quad (9)$$

From the mass balance, the concentration of the LS-form can be defined as a function of the concentration of the HS-form:

$$[\text{LS}]_t = [\text{HS}]_0 - [\text{HS}]_t \quad (10)$$

Eq. 9 becomes:

$$R_t = R_0 \times \frac{[\text{HS}]_t}{[\text{HS}]_0 - [\text{HS}]_t} \quad (11)$$

Combining Eq. 11 with Eqs. 4 and 5, R_t can be restated as a function of the double-integrated EPR signal of the HS-form:

$$R_t = R_0 \times \frac{a \times (A_{\text{HS}})_t}{(a \times (A_{\text{HS}})_0) - (a \times (A_{\text{HS}})_t)} = R_0 \times \frac{(A_{\text{HS}})_t}{(A_{\text{HS}})_0 - (A_{\text{HS}})_t} \quad (12)$$

This rearranges to:

$$h(t) = \frac{(A_{HS})_t}{(A_{HS})_0} = \frac{R_t}{R_0 + R_t} = e^{-k't} \quad (13)$$

$$\ln h(t) = -k' \times t \quad (14)$$

Plotting $\ln h(t)$ vs. t it is possible to extrapolate the quenching time of the process as intercept on the x-axis for $h(t) = 1$.

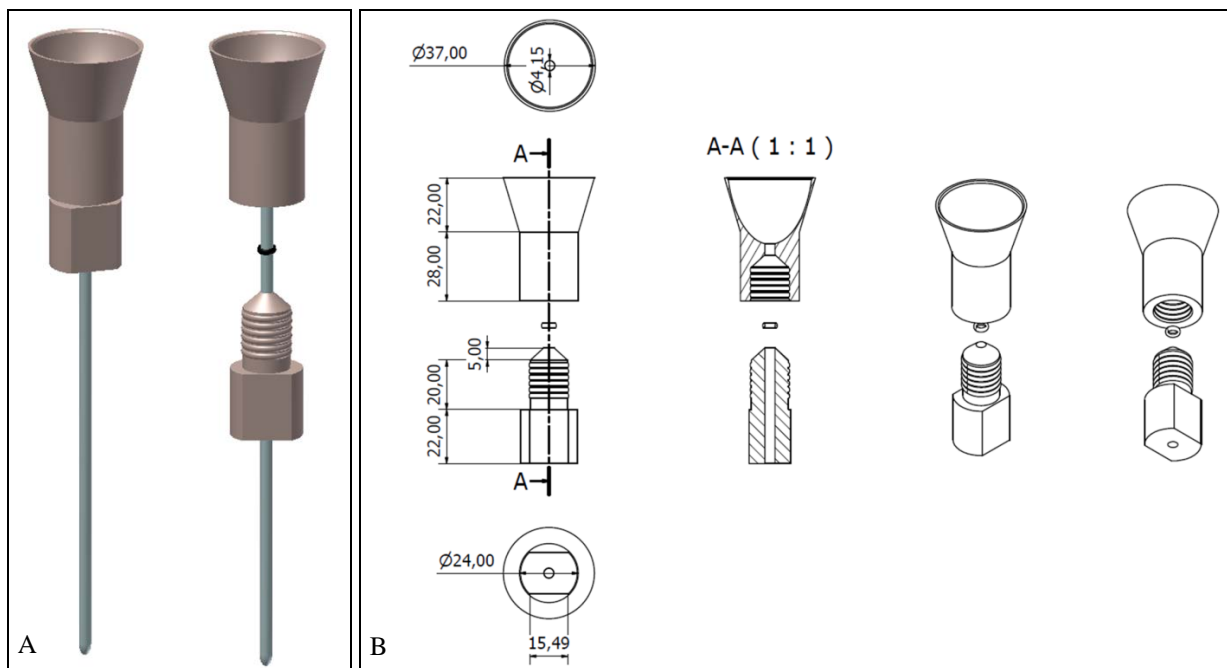


Figure S3: (A) 3D model presentation and (B) technical sketch of the sample collector used for analysis at X-band EPR (dimensions in mm).^[4] The sample collector is made in polytetrafluoroethylene (PTFE).

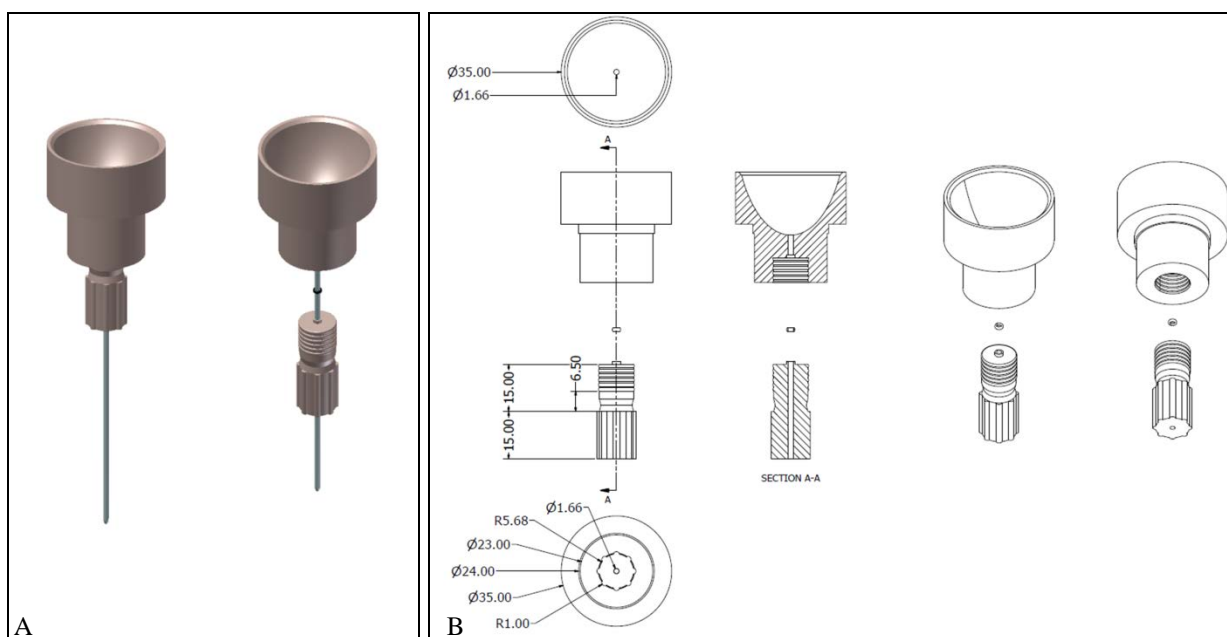


Figure S4: (A) 3D model presentation and (B) technical sketch of the sample collector used for analysis at Q-band EPR (dimensions in mm).^[4] The sample collector is made in polytetrafluoroethylene (PTFE).

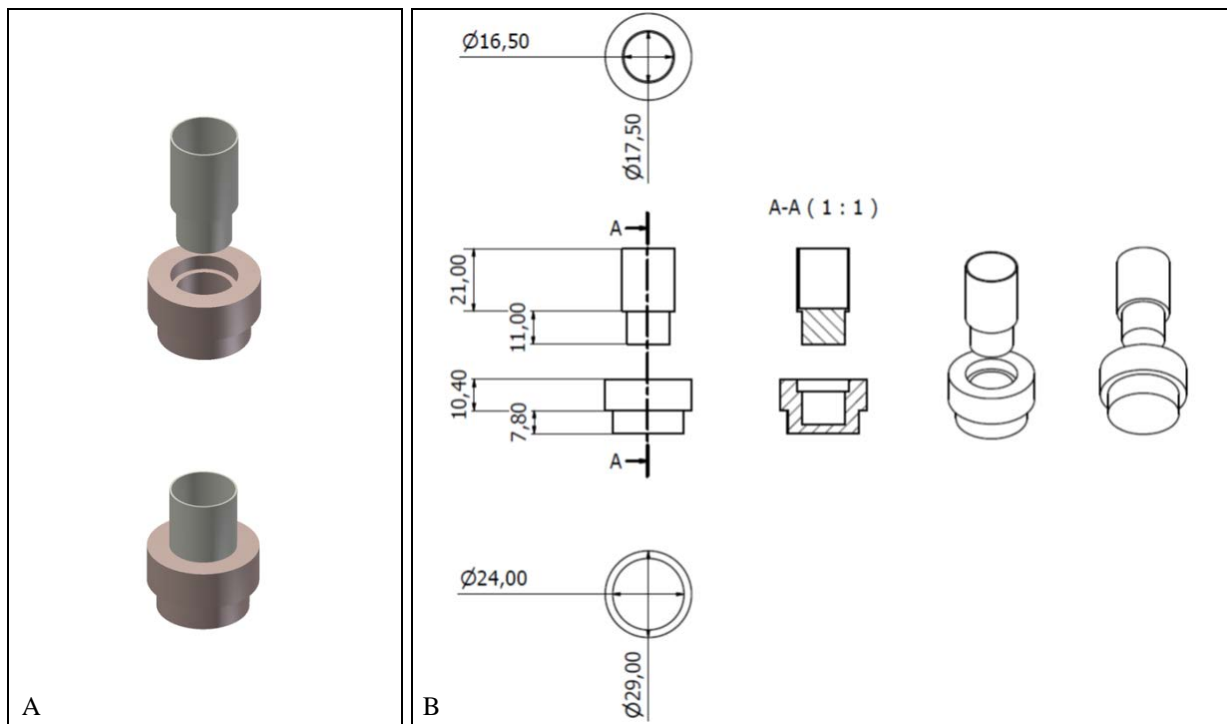


Figure S5: (A) 3D model presentation and (B) technical sketch of the sample collector used for analysis at W-band EPR (dimensions in mm).^[4] The smallest cylinder is made of polyisoprene and is embedded in the big metallic cylinder.

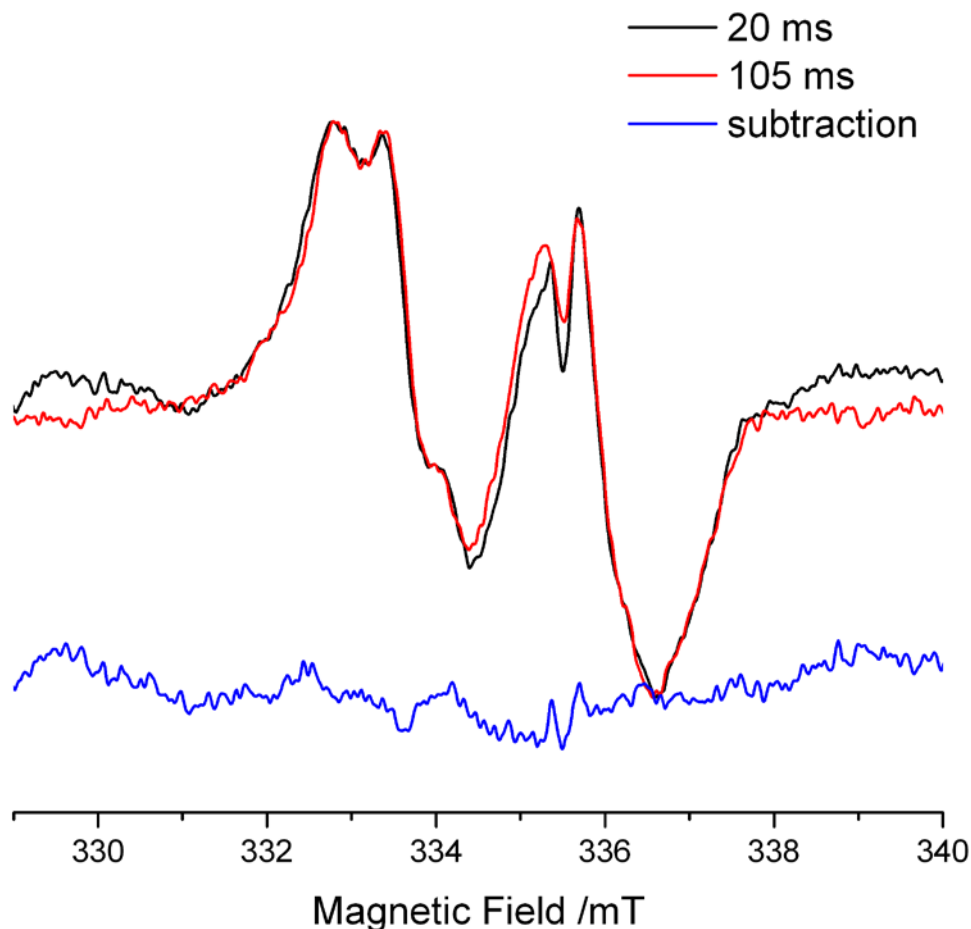


Figure S6: 9.4 GHz CW EPR of the radical formed after mixing of PpoA (100 μm) with 160-fold excess of (8*R*)-HPODE freeze quenched at 20 (black line) and 105 ms (red line), in small tubes (0.7 mm ID). The subtraction of the two spectra (in blue) clearly shows that the difference between the two spectra lies within the noise. EPR spectroscopic measurements were carried out using a Bruker Elexsys E500 CW-EPR and a Super-X microwave bridge operating at 9.3 - 9.5 GHz. The spectrometer was equipped with a standard Bruker X-band ER4119-SHQE cavity and a liquid helium cryostat (Oxford Instruments). Experimental parameters: $T = 70$ K, microwave power: 3.17 mW, conversion time: 30 ms, modulation amplitude: 4 G, modulation frequency: 100 kHz, 2 h signal averaging. To fit the cavity size of the resonator, the small tubes (0.70 mm ID) were inserted in a large tube (3 mm ID) before measurement.

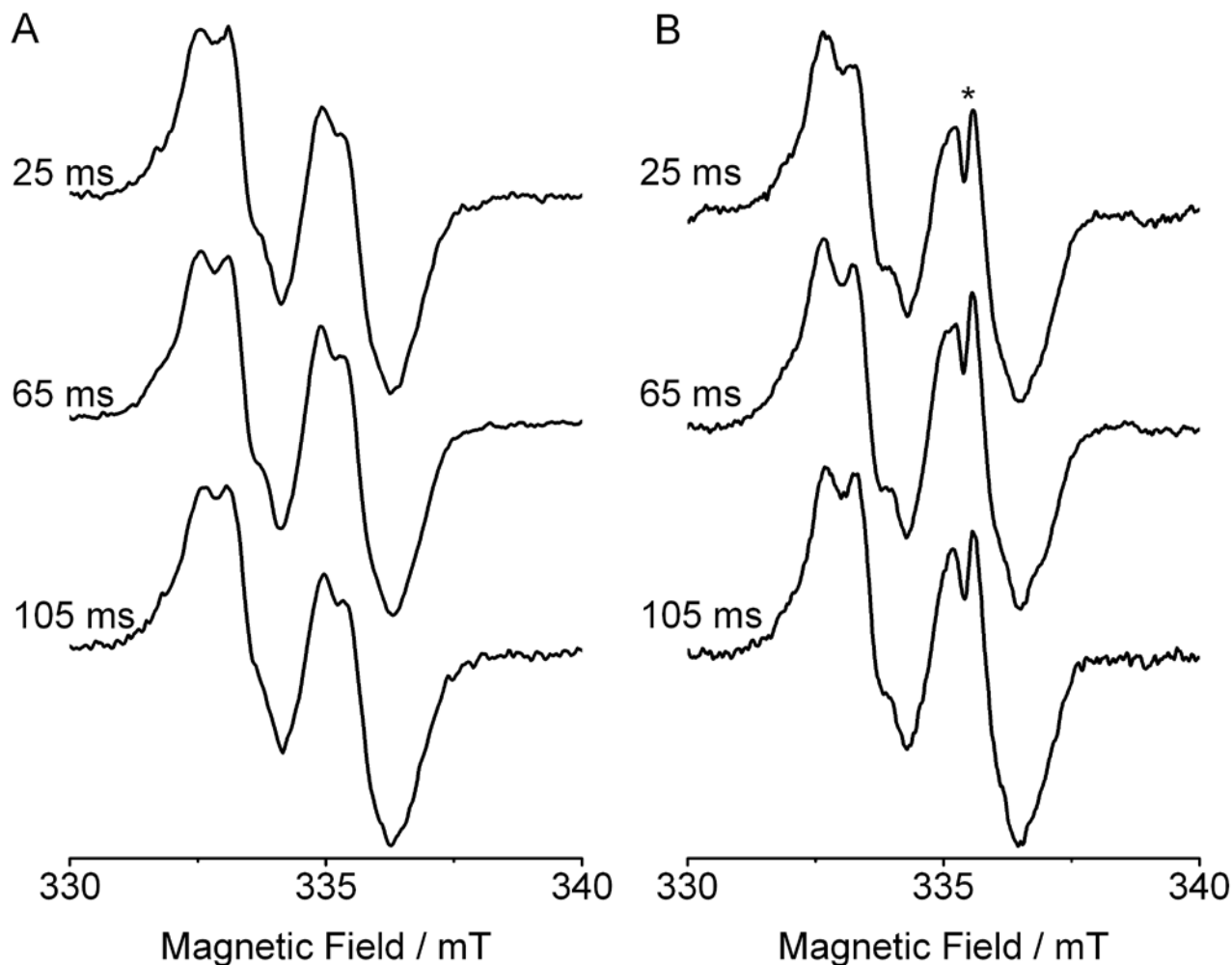


Figure S7: 9.4 GHz CW EPR of the radical formed after mixing of PpoA (100 μm) with 160-fold excess of (8R)-HPODE freeze quenched at different delay times in (A) large (3 mm ID)^[5] and (B) small tubes (0.7 mm ID). EPR spectroscopic measurements were carried out using a Bruker Elexsys E500 CW-EPR and a Super-X microwave bridge operating at 9.3 - 9.5 GHz. The spectrometer was equipped with a standard Bruker X-band ER4119-SHQE cavity and a liquid helium cryostat (Oxford Instruments). Experimental parameters: $T = 70$ K, microwave power: 3.17 mW, conversion time: 30 ms, modulation amplitude: 4 G, modulation frequency: 100 kHz, 2 h signal averaging for (B). To fit the cavity size of the resonator, the small tubes (0.70 mm ID) were inserted in a large tube (3 mm ID) before measurement. The signal marked with an asterisk is caused by a glass impurity.

References

- [1] H. Gutfreund, in *Methods in Enzymology*, Vol. 16 (Ed.: K. Kenneth), Academic Press, 1969, pp. 229-249.
- [2] A. L. Tsai, V. Berka, R. J. Kulmacz, G. Wu, G. Palmer, *Anal. Biochem.* 1998, 264, 165-171.
- [3] aJ. Blanck, W. Graf, W. Scheler, *Acta Biologica Et Medica Germanica* 1961, 7, 323-326; bD. E. Goldsack, W. S. Eberlein, R. A. Alberty, *J. Biol. Chem.* 1966, 241, 2653-2660.
- [4] The sample collectors was designed using Autodesk Inventor Professional (version 2012) software.
- [5] A. J. Fielding, F. Brodhun, C. Koch, R. Pievo, V. Denysenkov, I. Feussner, M. Bennati, *J. Am. Chem. Soc.* 2011, 133, 9052-9062.